university of groningen

faculty of science and engineering

Origin of the Baryonic j - M - f_{gas} relation

ASTRONOMY BACHELOR RESEARCH PROJECT

Elise Camilleri
S3944964

Supervisors:
Prof Dr F. Fraternali
Gabriele Pezzulli, PhD

July 8, 2022

Abstract

Galaxy scaling relations give important insight on the formation and evolution of galaxies by describing observable trends between their physical properties. One scaling relation of fundamental importance is that between a galaxy's baryonic mass (M_{bar}) and baryonic specific angular momentum (j_{bar}) for disc galaxies, the scatter of which has been shown to correlate with variations in the gas fraction (f_{gas}). This results in a tight linear relation between j_{bar}, M_{bar} and f_{gas}.

By assuming an exponential accretion profile in space and time, and assuming the standard Kennicutt-Schmidt (K-S) star formation law and a non-evolving baryonic Tully-Fisher relation (BTFR), we explore for the first time quantitatively whether the tight correlation between the j_{bar}, M_{bar} and f_{gas} can be explained, in a scenario of gas accretion, as a result of the star formation efficiency being lower in the outer regions of the galactic discs. The simple model developed throughout this thesis is described by the accretion timescale (t_{acc}) and radial scale-length of the accretion profile (r_{acc}). For a fixed M_{bar}, these two parameters are varied and an analysis of the variation induced in both j_{bar} and f_{gas} is conducted. We show that, given the assumptions of our model, r_{acc} is a suitable candidate to explain the observed correlation between f_{gas} and j_{bar} at fixed M_{bar}. Given that r_{acc} is related to the the angular momentum of the accreting gas, we speculate that this parameter could be the physical driver for the observed j_{bar} - M_{bar} - f_{gas} relation. Some limitations of the model are also discussed, as well as directions for future improvement.

Contents

1 Introduction

As an ever increasing amount of research is conducted in an attempt to understand the Universe and the laws that govern it, it is apparent that there exist various trends between galaxies' physical properties such as their mass, velocity and size. The existence of such relations gives information on galaxy formation and evolution, making studies concerning these relations of prime importance (e.g. Tully and Fisher (1977) ; S. M. Fall (1983) ; Kennicutt (1998); Fernández Lorenzo et al. (2011)).

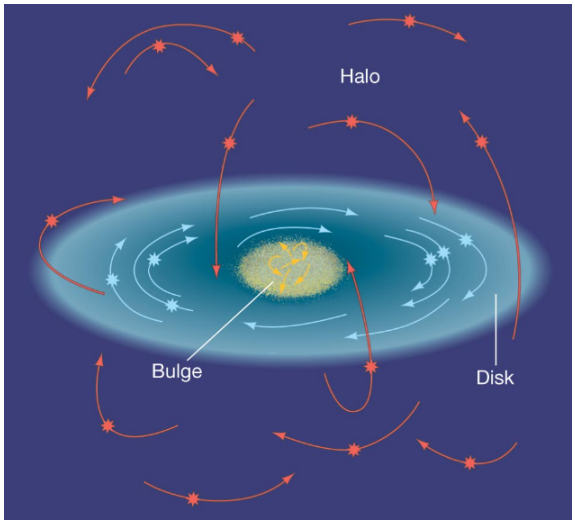

Figure 1: The spatial distribution and motions of the stars in the galactic bulge, disc and halo.

Based on their morphology, luminosity, chemical composition and mass, galaxies can be divided into various different types. However, the most common classification scheme used is the Hubble sequence, which is a morphological galaxy classification system developed by Hubble (1926). Within this classification scheme, the three main type of galaxies are the ellipticals, which are also referred to as early-type galaxies, spirals and irregulars which are both collectively referred to as late-type galaxies.

Spiral galaxies are composed of a central bulge, a relatively flat galactic disc, as well as stellar and dark matter (DM) halo. The spatial distribution and motions of stars in the various structures is represented in Figure 1. In turn, the galactic disc is composed of multiple components including gas, dust and stars, and their kinematics are governed dominantly by the gravitational force holding these components together. The various components interact through a multitude of physical processes. Stars form from the collapse of gas and dust under gravity, and they eject gas and dust back into the interstellar medium through the process of stellar feedback. This drives galactic fountains that produce the circulation of the gas between the disc and halo. At the same time new gas accretes onto the disc from the environment to feed star formation (e.g Kereš et al. (2009);

Fraternali (2017)).

Most of the star formation takes place in interstellar clouds within the galactic disc, and as a result, the disc is composed of a younger, brighter population of stars than those found in the bulge. Studies have also shown that the size of the stellar disc evolves and galaxy discs show an "inside-out" growth (e.g. Pezzulli et al. (2015)). Measuring this rate of growth gives insight on the physical processes of gas accretion and star formation as they drive the evolution of the gaseous and stellar galaxy components (Frankel et al. (2019)). Whilst both gas and stars are found within the galactic bulge and disc, their spatial distribution is different, in that within the disc, the gas is more extended than the stars. This can be attributed to a lower star formation efficiency in the outer parts of the galaxy discs.

In the twentieth century, through analysis of stellar and gas motions, spiral galaxy discs were discovered to be differentially rotating (Slipher (1913) ; P. van der Kruit and Allen (1978)). This led to intensive studies attempting to map the rotation curves of disc galaxies and the realisation that there appears to be "missing mass" in the galaxy which was later conceptualised in dark matter halos (e.g. van der Kruit and Bosma (1978) ; Faber and Gallagher (1979)).

Various studies have been conducted to understand the way in which the DM halo properties influence the formation and evolution of galaxies (e.g. Wechsler and Tinker (2018)) and thanks to the study of primordial nucleosynthesis and the cosmic microwave background (e.g. Pagel (1997) ; Komatsu et al. (2009)), the ratio of baryonic and DM is well understood. The amount of baryonic matter is known to make up approximately one-sixth of the total matter in the universe (Bennett et al. (2013)). In galaxies, the dark matter is found distributed within the galactic halo, which extends further out from the luminous bulge and disc, and is thought to play an important role in maintaining the stability of flattened disc galaxies (Ostriker and Peebles (1973)). Baryons and DM form the main ingredients of galaxy formation.

1.1 Galaxy Formation

In the currently accepted cosmological framework, the Universe is made of three main constitutents. These are the baryonic matter, the cold dark matter (CDM), in which "cold" refers to the fact that it moves at speeds much slower than the speed of light, and cosmological constant (Λ), which is related to dark energy. For this reason, the currently accepted cosmological model is also referred to by the term "ΛCDM", and the understanding is that in a ΛCDM universe, galaxies form and evolve within the extended gravitationally bound DM haloes (White and Rees (1978)).

1.1.1 Tidal Torque Theory

After dark matter halos collpased due to the growth of primordial overdensities, baryonic matter was later accreted onto these halos and, through radiative cooling, concentrated into the central regions, eventually leading to the formation of stars (Cimatti, Fraternali, and Nipoti (2019)). During this process the dark matter protohalo gains angular momentum as a result of the tidal torques that neighbouring structures exert on it. This is what is referred to as the tidal torque theory (TTT) and was proposed by Peebles (1969). The majority of the angular momentum of DM haloes is acquired during a stage at which the protohaloes are growing as a result of gravitational instabilities (López, Merchán, and Paz (2019)). The mass and specific angular momentum for the dark matter haloes are expected to scale according to the relation $j_h \propto M_h^{\frac{2}{3}}$ (Romanowsky and Fall (2012)).

Tidal torque theory can be used to make predictions about the angular momentum of galaxies, but this requires further assumptions. For instance, if the baryonic and dark matter experience the same torques, this results in the two having approximately equal specific angular momenta (j) which can be expressed as

$$j_{bar} = \frac{J_{bar}}{M_{bar}} \approx j_{DM} = \frac{J_{DM}}{M_{DM}}\,. \tag{1}$$

Here J_{bar} and J_{DM} represent the angular momenta of baryons and dark matter respectively, whilst M_{bar} and M_{DM} are the baryonic mass and dark matter mass (Cimatti, Fraternali, and Nipoti (2019)). In the absence of external influences, the angular momentum of gas is also conserved during the further collapse to the centre of the halo despite losing energy through radiation (S. Michael Fall and Efstathiou (1980)). Studying the specific angular momentum of baryons is extremely important in understanding how galaxies formed.

1.2 j - M relation

Among the most fundamental scaling laws for galaxies are the relations between a galaxy's specific angular momentum (j_i) and mass (M_i), where the i represents the stellar, the gaseous or their sum, the baryonic component. The importance of j and M comes from the fact that together the two parameters provide information about the dimensions, amount of material and rotational velocity of a galaxy. As a result, multiple studies looked at the j_i - M_i fundamental relations, as a tool to gain insights on the evolution of galaxy discs and spheroids (e.g S. M. Fall (1983) ; Obreschkow and Glazebrook (2014) ; Posti et al. (2020)).

Following the seminal work by S. M. Fall (1983) the j - M relation is also sometimes referred to as the Fall relation. After studying this for the stellar component, S. M. Fall (1983) observed that these two parameters are related by an unbroken power law, that in analogy to the expected law for dark matter, can be approxi-

mated as $j_* \propto M_*^{\frac{2}{3}}$, where j_* and M_* are the specific angular momentum and the mass of the stellar component respectively. This study also found that, disc galaxies and early type galaxies show very different normalisations (Romanowsky and Fall (2012)). The j - M relation has been the subject of numerous studies in recent years (e.g Obreschkow and Glazebrook (2014), Kurapati et al. (2018)) and its exact origin remains unknown and subject to investigation (e.g. Posti et al. (2020)).

For a sample of nearby disc galaxies, Mancera Piña et al. (2021) measured accurately the specific angular momentum of gas, stars and baryons, and analysed the corresponding j_i - M_i relation. The observations show that all these relations have a secondary dependence on the ratio between the gas mass (M_{gas}) and the baryonic mass (M_{bar}). This is referred to as the gas fraction (f_{gas}) and is given by

$$f_{gas} = \frac{M_{gas}}{M_{bar}} = \frac{M_{gas}}{M_{gas} + M_*}\,, \tag{2}$$

where M_{bar} is the summation of the gas (M_{gas}) and stellar mass (M_*). The tight $j - M - f_{gas}$ correlation found by Mancera-Piña et al. (2021) is given by the equation

$$\log\left(\frac{j_i}{kpc\ kms^{-1}}\right) = \alpha_i\ \log\left(\frac{M_i}{M_\odot}\right) + \beta_i\ \log\left(f_{gas}\right) + \gamma_i\,, \tag{3}$$

where i represents the stars, gas or baryons, and the coefficients of the best fit α, β and γ vary depending on galaxy component in question. Of the three relations, the baryonic relation was found to be the one with the smallest intrinsic scatter and therefore is arguably the most fundamental of the three.

The study showed that a higher gas fraction corresponds to larger value for the stellar, and baryonic specific angular momenta for a fixed M_* or M_{bar}, whilst the opposite is true for the gas. This behaviour can be described by planes given by equation 3 whose projections at fixed f_{gas} are shown in Figure 2. Following their observations, Mancera-Piña et al. (2021) proposed that a qualitative explanation can be related to the observation that the gas is distributed at larger radii than the stars due to the star formation efficiency being lower in these regions. This research project aims to continue on the work by Mancera-Piña et al. (2021) and explore this idea of star formation efficiency in a more quantitative way.

1.3 Aim of this work

This bachelor thesis aims to explore analytical models that constitute a first step towards a possible explanation of the relation between the baryonic mass (M_{bar}) and the baryonic specific angular momentum (j_{bar}) with the inclusion of gas fraction (f_{gas}). In particular, I have considered a simple galaxy evolution model where gas accretion is described by two parameters: the accretion timescale (t_{acc}) and the radial scale length of the accretion profile (r_{acc}). The main aim is to investigate how f_{gas} and j_{bar} respond to changes in the assumed r_{acc} and t_{acc} for

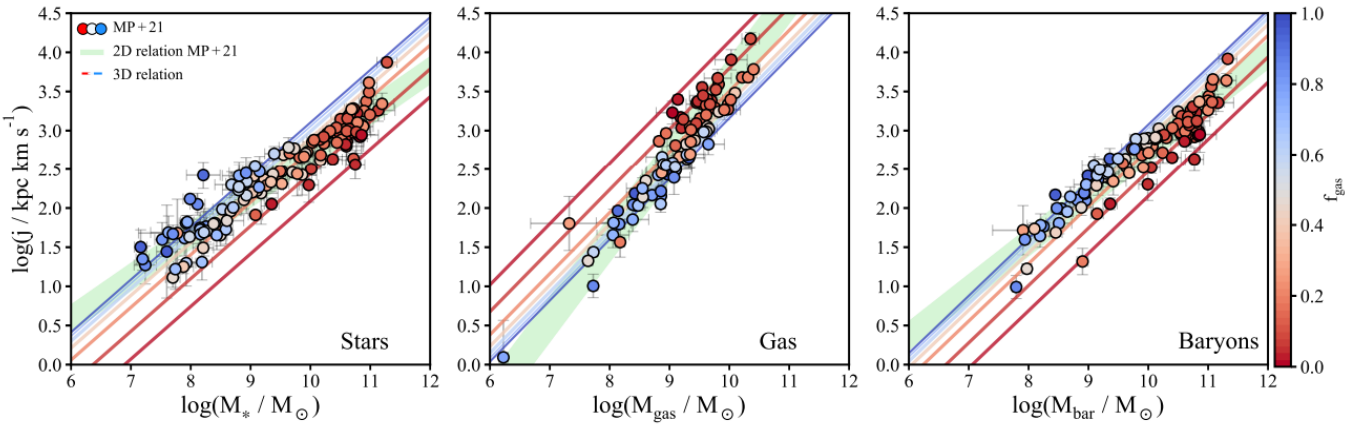

Figure 2: Observed relations between stellar, gas and baryonic mass and their respective specific angular momentum. Each data point is color coded depending on its gas fraction. Six lines with constant f_{gas} are overlayed on the points having values of 0.01, 0.05, 0.2, 0.4, 0.6, 0.8 ranging from red to blue. Taken from Mancera-Piña et al. (2021)

a range of baryonic masses. In creating the model, existing scaling relations will be used and assumptions concerning their evolution will be made. These include the Kennicutt–Schmidt law (Section 2.1), the relation between the baryonic mass (M_{bar}) and stellar disc size (R_d) (Section 2.3) and the baryonic Tully-Fisher relation (Section 2.6).

In Section 2, the research methods used to create our galaxy evolution model will be presented, including the various assumptions made and the motivation behind them. Following this, the results obtained and the comparison of the model with observations will be shown in Section 3. The findings as well as the limitations and possible future work will be discussed in Section 4, followed by a summary and conclusions in Section 5.

2 Research Methods

In this research project, the j_{bar} - M_{bar} relation with the inclusion of the gas fraction (f_{gas}) was investigated in an attempt to explain it quantitatively. This was done by building a simple galaxy evolution model based on the assumption of having an exponential accretion history and following the Kennicutt–Schmidt star formation law. The following subsections will explain the assumptions made and the steps taken in creating the model.

2.1 Star Formation Laws

Star formation laws attempt to describe the strong correlation observed between the amount of gas the galaxy possesses and the rate at which this gas collapses to form stars (Kennicutt and Evans (2012) ; Zonoozi et al. (2021)). One of the most commonly used star formation law is the Kennicutt–Schmidt (K-S) law which was initially proposed by Schmidt (1959). It deals with surface densities and relates that of the star formation rate (SFR) to the gas surface density by the power law

$$\Sigma_{SFR} = A\,\Sigma_{gas}^{N} \tag{4}$$

where A and N are constants. Throughout this research project it was assumed that the star formation law that galaxies follow is the K–S law, but in Section 4.2.3 a different law will also be explored. The values of parameters N and A in equation 4 were found by Kennicutt (1998), and for surface densities measured in $M_{\odot}pc^{-2}$, and time in Gyr they have a value of 1.4 and 0.1625, respectively. Here, the constant A includes within it a correction for interstellar helium (G. Pezzulli and Filippo Fraternali (2016)).

The gas and star surface densities denoted by Σ_{gas} and Σ_{*} respectively were taken to evolve in time according to:

$$\frac{d\,\Sigma_{gas}}{dt} = \dot{\Sigma}_{acc} + \dot{\Sigma}_{fb} - \Sigma_{SFR} \tag{5}$$

$$\frac{d\,\Sigma_{*}}{dt} = \Sigma_{SFR} - \dot{\Sigma}_{fb}\,, \tag{6}$$

where the subscript "fb" stands for stellar feedback, meaning the rate at which stars return gas back to the interstellar medium throughout their evolution (Tinsley (1980)). As a result, $\dot{\Sigma}_{fb}$ is the surface density of the rate of stellar feedback. Σ_{SFR} is the surface density of the star formation rate and $\dot{\Sigma}_{acc}$ is the sur-

face density of the rate of gas accretion (Filippo Fraternali and Tomassetti (2012)). Throughout this project a timescale between 0 to 12 Gyr was used, where 0 Gyr represents the time when the galaxy is assumed to begin its formation whilst t_o =12 Gyr is taken to be the present day. This particular timescale, as opposed to the age of the universe, was used since the focus of this thesis is only on the disc component of the galaxy, and, although there is some debate on the subject, it is commonly believed that the formation of the disc starts with some delay (Cimatti, Fraternali, and Nipoti (2019)).

The instantaneous recycling approximation (IRA) was then used to simplify equations 5 and 6 into:

$$\frac{d\,\Sigma_{gas}}{dt} = \dot{\Sigma}_{acc} - \Sigma_{rSFR} \tag{7}$$

$$\frac{d\,\Sigma_{*}}{dt} = \Sigma_{rSFR}. \tag{8}$$

This approximation states that all stars less massive than one solar mass have an infinite lifespan, whilst stars more massive than this end their life cycle instantaneously (Prantzos (2008)). As a result, for every time value, the mass fraction returned back to the interstellar medium by the newly formed stars is a constant known as the return factor ($\mathcal{R}$) and the surface density of the rate of stellar feedback ($\dot{\Sigma}_{fb}$) can be replaced by $\mathcal{R}\,\Sigma_{SFR}$ (Filippo Fraternali and Tomassetti (2012)). Σ_{rSFR} is then the surface density of the reduced Star Formation Rate when taking the IRA into account and is defined by $\Sigma_{rSFR} = \Sigma_{SFR}(1 - \mathcal{R})$.

The return factor is dependent on how the star masses are distributed within a population at the time of its formation which, in turn, can be described empirically in terms of an initial mass function (IMF). To date, various different IMFs have been proposed in the literature. These include the Kroupa (Kroupa, Tout, and Gilmore (1993)), Chabrier (Chabrier (2003)) and Salpeter IMF (Salpeter and Bethe (1951)). Following the paper by Filippo Fraternali and Tomassetti (2012) the stars in this model were assumed to follow a Salpeter initial mass function, and as a result, the return factor was taken to have a value of 0.30. However, having adopted the different assumptions proposed by the Kroupa or Chabrier IMFs would not have made a significant difference in any results obtained as within the assumptions of this thesis, these two give a return factor of 0.31 and 0.32, respectively (Chabrier (2003)).

2.2 Accretion History

In this bachelor's research project, it is assumed that the gas accretion rate surface density is exponential in both time and distance from the center of the galaxy. Also, the time and radial dependence are independent of each other such that the

two can be treated separately. We can write the accretion rate surface density as follows:

$$\dot{\Sigma}_{acc}(t, R) = \frac{\dot{M}_{acc}(t)}{2\,\pi\, r_{acc}^2}\, e^{-\frac{R}{r_{acc}}}\,, \tag{9}$$

where the subscript "acc" seen in equation 9 stands for "accretion", r_{acc} is the radial scale-length of the accretion profile and $\dot{M}_{acc}$ is the accretion rate given by the equation

$$\dot{M}_{acc}(t) = Ce^{-\left(\frac{t}{t_{acc}}\right)}\,. \tag{10}$$

The surface density of all the material that was accreted between time 0 Gyr, i.e. at the beginning of the formation of a galaxy, and an arbitrary time "t" at a given radius "R" is given by

$$\Sigma_{acc}(t, R) = \int_0^t \dot{\Sigma}_{acc}(t', R)\,\mathrm{d}t' = \Sigma_{bar}(t, R)\,. \tag{11}$$

Equation 11 shows how, in the absence of outflows or internal motions such as radial gas flows, the surface density of accreted matter is equivalent to surface density of baryons at time t. As a result, the total accreted mass is the same as the the baryonic mass (M_{bar}) and is expressed by

$$M_{bar}(t) = \int_0^t Ce^{-\left(\frac{t'}{t_{acc}}\right)}\,\mathrm{d}t'\,, \tag{12}$$

where t_{acc} is the accretion timescale.

Since in this model the galaxy is accreting gas from the intergalactic medium, the total baryonic mass (M_{bar})of the galaxy is not constant, but will increase with time up to a particular known value at t_o. After integrating in time equation 12, the relation can be inverted to determine the constant C that gives a desired value for the baryonic mass at a given time t. For $t = t_o$, C is defined as

$$C = \frac{M_{bar}(t_o)}{t_{acc}\,\left[1 - e^{-\left(\frac{t_o}{t_{acc}}\right)}\right]}\,. \tag{13}$$

Substituting t_o = 12 Gyr, a range of values of M_{bar} in units of $M_\odot$ and the desired accretion timescale needed to be analysed, corresponding values for the constant C were determined according to equation 13.

The two parameters r_{acc} and t_{acc} are the main focus of this work as the aim is to study how variations in these parameters influence the $M_{bar} - j_{bar} - f_{gas}$ relation.

More specifically, this work aims to investigate whether changes in one or both of the parameters, whilst keeping a fixed baryonic mass, induce any variation in j_{bar} and f_{gas} making them correlated as observed in real galaxies by Mancera-Piña et al. (2021). This was done by exploring three different values for the accretion timescale, namely 3, 10 and 25 Gyr, and determining values for r_{acc} by making assumptions using existing galaxy scaling relations.

2.3 Mass Size Relation

In determining a value for r_{acc}, a scaling relation between baryonic mass and stellar disc scale-length as defined by Wu (2018) was used. In the study conducted by Po-Feng Wu, it was concluded that the baryonic mass, denoted by M_{bar} and the size of the stellar disc are related by

$$\log\left(\frac{R_*}{kpc}\right) = 0.385\left[\log\left(\frac{M_{bar}}{M_\odot}\right) - 10\right] + 0.281\,, \tag{14}$$

where R_* is the scale-length of the stellar disc. Equation 14 was then used to determine a value for r_{acc} for each corresponding value of M_{bar}. Taking the assumption that r_{acc} is equivalent to R_* as defined by Wu is not perfect since, as will be seen at a later stage, the stellar disc in our model is not an exact exponential. However, there are no direct observations of r_{acc}, and so this assumption is made in order to simplify the computation as well as to obtain credible results as a first step in creating a galaxy evolution model. For a constant baryonic mass, the relation in equation 14 has a significant scatter of $\sim$0.18 dex in scale-length.

I have considered 50 values for the baryonic mass ranging from $10^8 M_\odot - 10^{11.5} M_\odot$, the corresponding range of values of r_{acc} were determined using the relation in Wu (2018). This range of masses was chosen specifically to be identical to that in the study by Mancera-Piña et al. (2021), so that direct comparison could be made between the results obtained and the observations. For each baryonic mass considered, the fiducial value of r_{acc} was determined using equation 14. This nominal value was then divided and multiplied by two and a range of ten values of r_{acc} were explored by setting these two numbers as the lower and upper limit respectively.

2.4 Evolution of the gas and star surface density

After having defined the accretion history as the starting point of this model, chosen three values for t_{acc}, and derived r_{acc} and values for C, the next step was to derive the surface gas density (Σ_{gas}) and the surface star density (Σ_*) using equations 7 and 8. To do this, the Kennicutt–Schmidt law was used and by substitut-

ing equation 4 into equation 7 the following equation 15 for Σ_{gas} was obtained analytically:

$$\frac{d\,\Sigma_{gas}(t,R)}{dt} = \frac{C}{2\,\pi\,r_{acc}^2}\,e^{-\frac{t}{t_{acc}}}\,e^{-\frac{R}{r_{acc}}} - A\,(1-\Re)\;\Sigma_{gas}^{N}(t,R)\,. \tag{15}$$

This was then solved numerically, using the Runge Kutta method. Here, equation 15 was integrated in time from 0 to 12 Gyr, and an initial starting value for Σ_{gas} was taken to be 0 at every radius.

Once values for Σ_{gas} were obtained, Σ_* was then found using two different methods. This was done purely to ensure that the results obtained are in agreement with each other and hence double check that no mistake was done in carrying out the numerical calculations. The first method was using equation 8 together with the Kennicutt–Schmidt law. Integrating the equation obtained in time leads to

$$\Sigma_*(t,R) = A\,(1-\Re)\int_0^t \Sigma_{gas}^{N}(t',R)\mathrm{d}t'\,. \tag{16}$$

The integration was carried out from time t = 0 to t = 12 Gyr using Simpson's method. The second method was using equation 11 to derive Σ_{bar}, and then obtaining the surface density of stars by subtracting Σ_{gas} from Σ_{bar}:

$$\Sigma_*(t,R) = \Sigma_{bar}(t,R) - \Sigma_{gas}(t,R) = \int_0^t \frac{C}{2\,\pi\,r_{acc}^2}\,e^{-\frac{t'}{t_{acc}}}\,e^{-\frac{R}{r_{acc}}}\,\mathrm{d}t' - \Sigma_{gas}(t,R)\,. \tag{17}$$

Both calculations yielded the exact same result.

2.5 Masses and Gas Fraction

Integrating over radius the surface densities of gas and stars calculated as explained in Section 2.4 would then yield the total mass for both components of the disc. This can be written

$$M_i\,(t) = 2\,\pi\int_0^{R_{max}} \Sigma_i\,(t,\,R)\;R\,\mathrm{d}R\,, \tag{18}$$

where the subscript "i" can be replaced by stars, gas or baryons depending on which of the three is needed to be analysed. I have set $R_{max} = 100kpc$ after verifying that it was large enough to reach convergence.

Once masses were obtained, the gas fraction was calculated using the equation $f_{gas} = \frac{M_{gas}}{M_{bar}}$, where the baryonic mass is the summation of the gas and stellar mass.

2.6 Specific Angular Momentum

Following the above, the specific angular momentum was next to be determined. This quantity is defined as the angular momentum divided by the mass, according to the equation $j_i = \frac{|J_i|}{M_i}$, where once again i can represent the gas, star or baryonic component. Using explicit expressions for the angular momentum and mass in terms of the surface densities yields the following equation (Posti et al. (2018)):

$$j_i(t) = \frac{\int_0^{R_{max}} v_{rot}(R)\,\Sigma_i\,(t,\ R)\ R^2\,\mathrm{d}R}{\int_0^{R}\Sigma_i\,(t,\ R)\ R\,\mathrm{d}R} \tag{19}$$

where R is the radius measured from the galactic center and v_{rot} represents the rotation velocity which we assume to be the same for stars and gas. The observed trend is for the stellar v_{rot} to lag behind that of the gas; a phenomenon known as an asymmetric drift and as a result, oppositely to the model created in this research project, stars and gas have a different v_{rot} in reality. However, Posti et al. (2018) estimated this correction to be smaller than 10% in j_{bar}, and so taking the v_{rot} to be equivalent for gas and stars was sufficient.

In calculating the specific angular momentum by using equation 19, values for the rotational velocity (v_{rot}) needed to be established. This was done by making two types of assumptions. The first assumption was done by taking the rotational velocity to be constant in R, hence it is assumed to change only with time. This is a simplifying assumption because although in reality the rotational velocity varies with radius, taking it to be constant would greatly simplify the calculations whilst introducing a relatively small error (Romanowsky and Fall (2012)). This is because of the factor R^2 in the numerator of equation 19, implying that the dependency of the rotational velocity on the outer part of the galaxy is of more importance than the dependency on the inner part. Since at a larger radius, the rotational velocity is more or less constant, then the assumption that v_{rot} is constant in radius is valid (Vukcevic (2021)). The second assumption was that v_{rot} can be derived from the baryonic Tully-Fisher relation (BTFR) and that this not evolving with time. We assume in particular the expression derived by McGaugh (2012):

$$M_{bar} = A_G\, v_{rot}^4 \tag{20}$$

where A_G has a value of $47 \pm 6 M_\odot\, km^{-4}\, s^{-4}$. The BTFR creates a connection between the maximum rotational velocity, which is a property of dark haloes, to the luminosity or baryonic mass of the galaxy disc. The assumption that the relation does not evolve with time is a physical assumption as to date it is not known

whether galaxies evolve according to the BTFR at all redshifts or not. However some studies have shown that at least the stellar Tully–Fisher relation has not evolved significantly since z$\sim$1 (e.g. Teodoro, F. Fraternali, and Miller (2016)). Using equation 20 taken from the work by McGaugh (2012), a value for the rotational velocity was found, corresponding to each value of the baryonic mass. The evolution of v_{rot} in our model, comes from the fact that this is parameter is related to M_{bar} in accordance to equation 20, and M_{bar} evolves as a consequence of gas accretion.

The above calculations for the gas fraction and specific angular momentum were conducted multiple times for different values of the parameters and experimenting to see how the $M_{bar} - j_{bar} - f_{gas}$ relation changes as a result of these variations. The first approach was to vary t_{acc} whilst keeping r_{acc} constant at a nominal value as obtained using the relation between baryonic mass and stellar disc scale-length by Wu (2018), as explained in Section 2.3. The second approach was to keep the accretion timescale constant whilst varying the radial scale length of the accretion profile. In this second case, r_{acc} was varied between one half and twice the value indicated by the relation of Wu (2018) (as also explained in Section 2.3).

3 Results

3.1 Illustrative model

To illustrate the main properties of the model, I show in some detail the results for one example taking the present day baryonic mass to be $M_{bar} = 10^{10} M_{\odot}$.

3.1.1 Gas and Star Surface Densities

Following the method described in Section 2.4, equations 15 and 16 were used to create plots for Σ_{gas} and Σ_* against time. This particular example was done by taking $M_{bar}(t_0) = 10^{10} M_{\odot}$ and $r_{acc} = 1.9kpc$ following equation 14. The results shown in Figure 3 are for three values of t_{acc} =3, 10 and 25Gyr at the center of the galaxy (r=0).

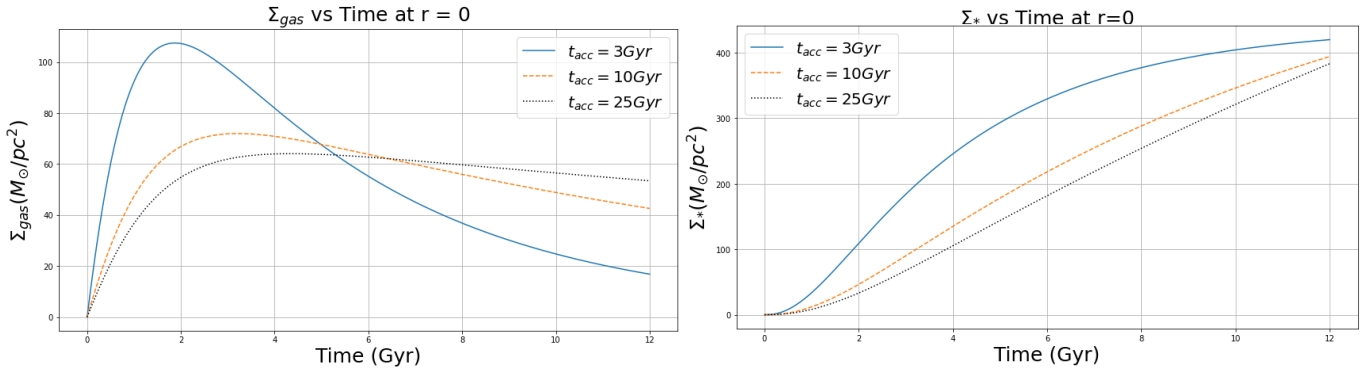

(a) Central gas surface density versus time

(b) Central star surface density versus time

Figure 3: Surface densities for gas (3a) and stars (3a) against time for a model with $M_{bar}(t_0) = 10^{10} M_{\odot}$. Three different accretion timescales of 3, 10 and 25 Gyr were considered and the radius was set to 0.

As can be seen from the plots, the surface density of gas starts off at 0 in the beginning. By the K-S law this then implies that the star formation rate also starts from zero and we also see that in Figure 3b the stellar mass surface density begins at 0 when time is 0 Gyr. The Σ_{gas} first increases and reaches a maximum depending on the accretion timescale. The peaks in Σ_{gas} seen in Figure 3a corresponds to the steepest part in Σ_* observed in Figure 3b, since it is at this time that star formation is at its maximum. The shorter the accretion timescale the quicker this maximum is reached and the more steeply Σ_{gas} declines following this point.

The plot for Σ_* (3b) shows that the smaller the value for t_{acc} the steeper the increase in Σ_* is initially. As a result the time taken for half the stars to form in this model is the shortest for an accretion timescale of 3 Gyr, and this increases

with increasing t_{acc}. In the galactic center this value increases from 3.39Gyr, for t_{acc} =3 Gyr to 6.27 Gyr, for t_{acc} =25 Gyr.

In Figure 4 we show the logarithm of the surface densities against radius for models with t_{acc} =10 Gyr.

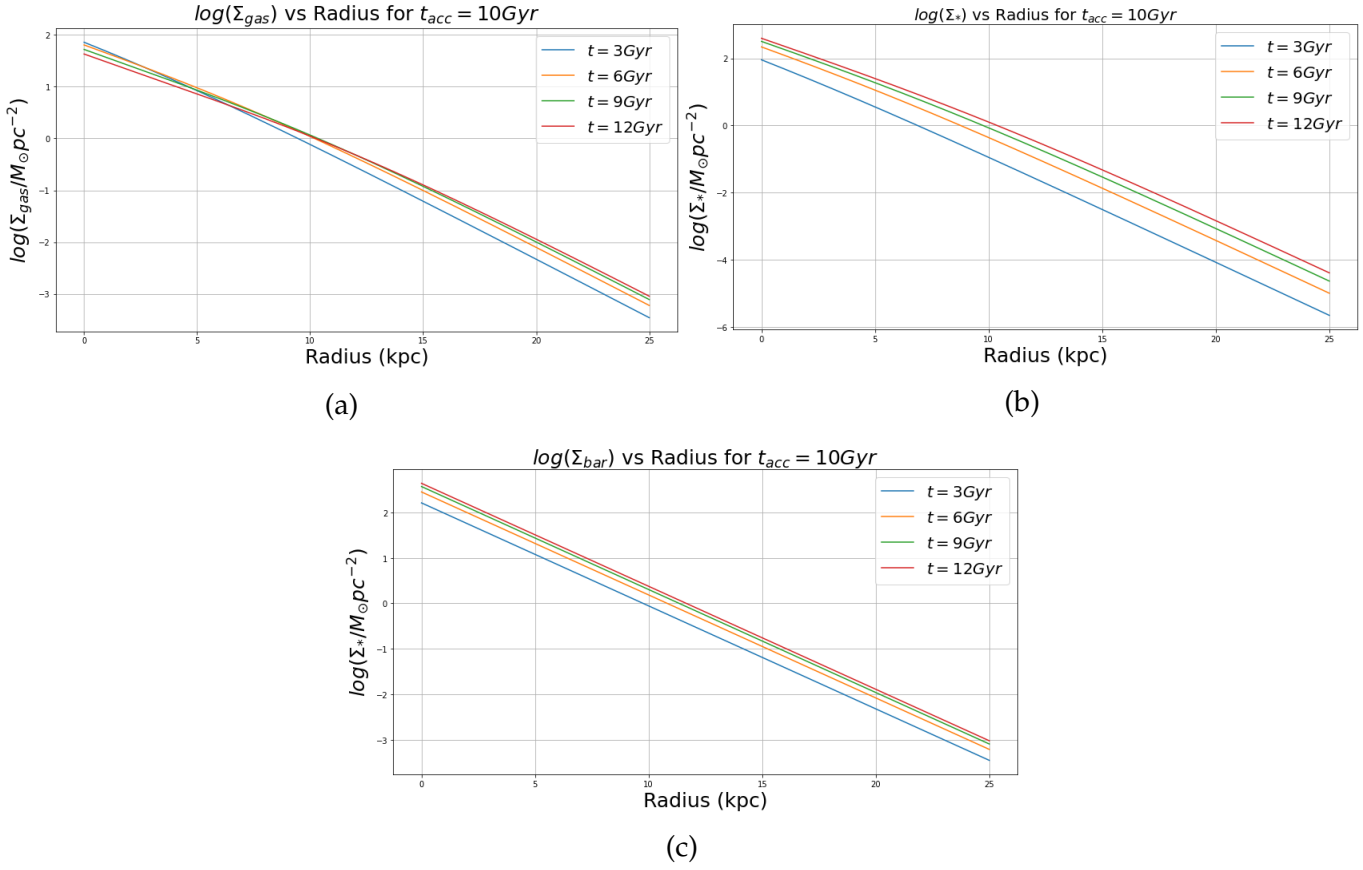

Figure 4: surface densities for gas (4a), stars (4b) and baryons (4c) in the logarithmic scale against radius for four representative values in time. The graphs above are for an accretion timescale of 10 Gyr

As a consequence of the exponent N > 1 in the K-S Law (equation 4), stars and gas are distributed differently from each other, and both deviate from an exponential. However, their summation (Σ_{bar}) has constant a scale length with time. As a result, by plotting log(Σ) against radius for different values of time under our current assumption, we see that only the total surface density (Σ_{bar}) is a perfect exponential with with constant scale length (Figure 4c). The same property is valid for all accreting timescales t_{acc}.

In plot 4c we see that at larger time values, Σ_{bar} the normalisation changes more slowly since most gas is accreted in the beginning. Whilst different accretion timescales show the same trend, as t_{acc} increases we also see more variation in Σ_{bar} at late times, as gas is accreted later. For the accretion timescales of 3 and 25 Gyr, a similar trend was observed as that shown in Figure 4 for t_{acc} = 10Gyr.

However, as expected, the smaller the accretion timescale, the smaller the range in normalisation at later times and so in plots for log(Σ_{bar}) against radius, Σ_{bar} changes less for $t_{acc} = 3$Gyr than for $t_{acc} = 25$Gyr. This is shown in Figure 5

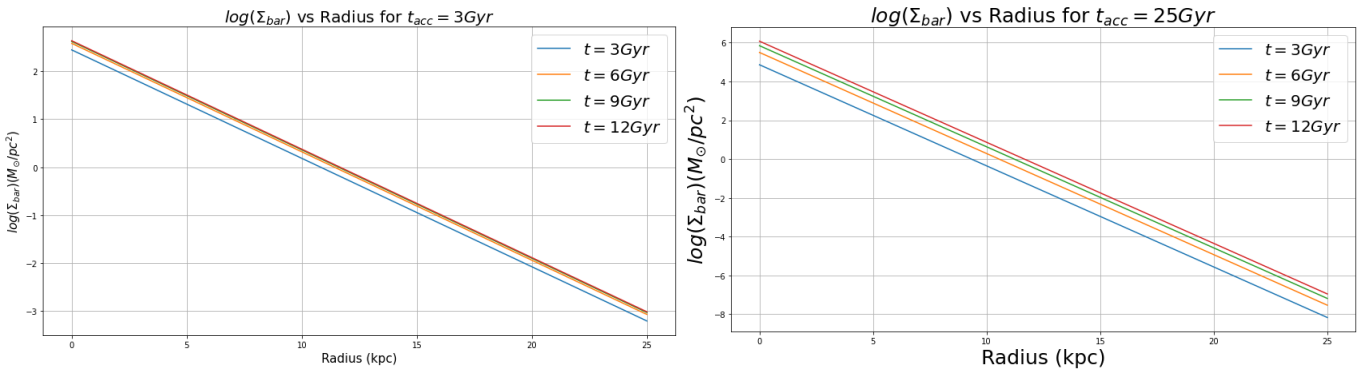

(a) (b)

Figure 5: Baryonic surface density in the logarithmic scale against radius an accretion timescale of 3Gyr (5a) and 25Gyr (5b).

From the surface densities, the gas, star and baryonic masses were determined as described in Section 2.5 using equation 18. These were then plotted against time and radius, and, to study the convergence of the integral, also against the maximum radius R_{max}. Figure 6 shows the gas and stellar cumulative mass against radius for an accretion timescale of 3 Gyr. These graphs enabled the determination of the upper limit for radial integrations. Since the cumulative masses are converged at 25kpc, all integrations in radius, for this particular example of $M_{bar}(t_0) = 10^{10} M_{\odot}$, could be stopped at this value. The graphs for an accretion timescale of 10 and 25 Gyr showed the same trend as that seen in Figure 6 where the masses increase from 0 up to a value and can be assumed to remain unchanging beyond 25kpc. However, for other models with higher mass and radial scale-length, we found that R_{max} = 25 kpc was insufficient and therefore we integrated up to R_{max} = 100 kpc.

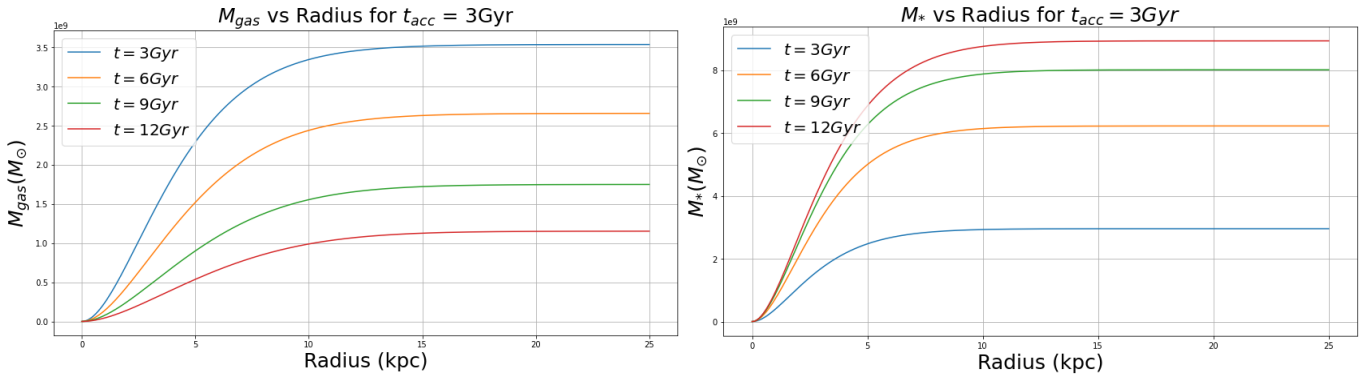

(a) Gas cumulative mass versus radius

(b) Star cumulative mass versus radius

Figure 6: Two plots showing the gas cumulative mass (6a) and stellar cumulative mass (6a) against radius for four representative times. The graphs above are for an accretion timescale of 3 Gyr

At t = 12 Gyr, summing up the gas and stellar mass yields the baryonic mass of $10^{10} M_\odot$ which was assumed for this example. Later on, a range of values for the baryonic masses at 12 Gyr will be considered.

3.1.2 Local Gas Fraction and SFE

The local gas fraction at each radial distance was plotted following the equation $f_{gas}(r) = \frac{\Sigma_{gas}(r)}{\Sigma_{bar}(r)}$ and can be seen in Figure 7.

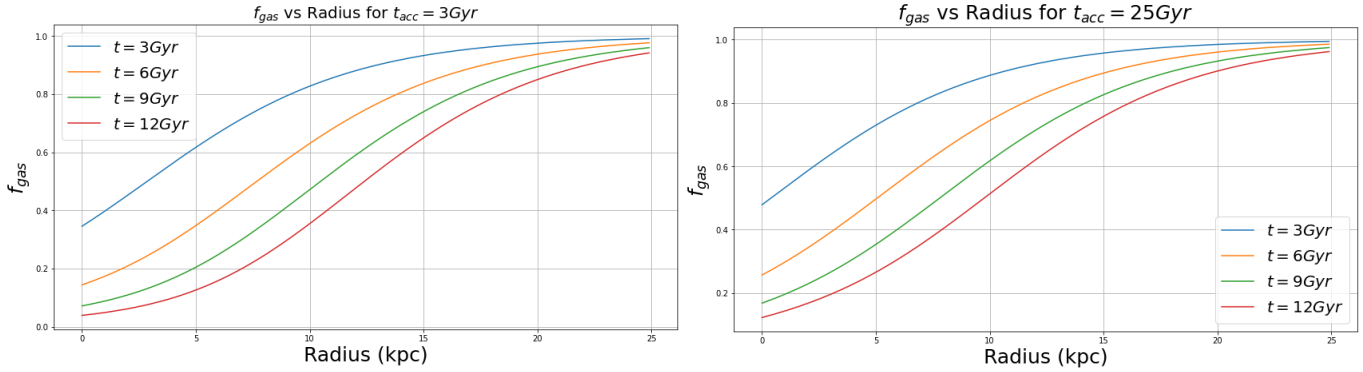

(a) Gas fraction versus radius for $t_{acc} = 3Gyr$

(b) Gas fraction versus radius for $t_{acc} = 25Gyr$

Figure 7: Gas fraction against radius for our illustrative model with $M_{bar}(t_0) = 10^{10} M_\odot$. The plots are for the accretion timescales of 3 Gyr (7a) and 25 Gyr (7b) at four representative times.

Figures 7a and 7b show how the gas in this particular model is more extended than the stars. In the outer regions, f_{gas} is observed to increase, and although

not shown, a similar trend was observed also for t_{acc} = 10 Gyr. This behaviour is a consequence of the low star formation efficiency in outer regions, resulting in more gas mass present in these regions with respect to the stellar mass. The star formation efficiency (SFE) is the ratio of surface densities of the star formation rate (SFR) and that of the gas, and its inverse is the timescale to convert gas into stars. Hence in my model since the K-S law was used, the SFE can be written

$$SFE = \frac{\Sigma_{SFR}}{\Sigma_{gas}} = A\,\Sigma_{gas}^{N-1}\,. \tag{21}$$

From equation 21, for N > 1, as is the case in my model, the SFE increases depending on Σ_{gas}. Hence taking a value of N = 1.4 was crucial to this model and at the outer regions of a galaxy, the gas is converted into stars with a larger timescale resulting in the highest f_{gas} at 25kpc.

The different accretion timescales produce slight differences in the gas fraction. For $t_{acc} = 3$Gyr the value of f_{gas} at early times is lower than that for $t_{acc} = 25$Gyr since for a lower t_{acc}, the galaxy is accreting gas at a faster rate. This induces a higher gas surface density and following equation 21, it results in a higher SFE which leads to a lower gas to star ratio. However, plots 7a and 7b show two extreme t_{acc} and yet the effect of varying t_{acc} on f_{gas} for $M_{bar}(t_0) = 10^{10} M_\odot$ is moderate.

3.2 Varying the accretion timescale : Observing the Effect on f_{gas} and j_{bar}

As discussed in Section 2 , the first approach taken in an attempt to understand the $M_{bar} - j_{bar} - f_{gas}$ relation was to investigate how the global values of f_{gas} and j_{bar} respond to variations in t_{acc} for fixed $M_{bar}(t_0)$ and fixed r_{acc}. As in Section 3.1, $M_{bar}(t_0)$ was taken to be $10^{10} M_\odot$ and $r_{acc} = 1.9kpc$. Taking accretion timescales of 3, 10 and 25 Gyr, plots for the global gas fraction and specific angular momentum against time were obtained following the description in Sections 2.5 and 2.6, and can be seen in Figure 8.

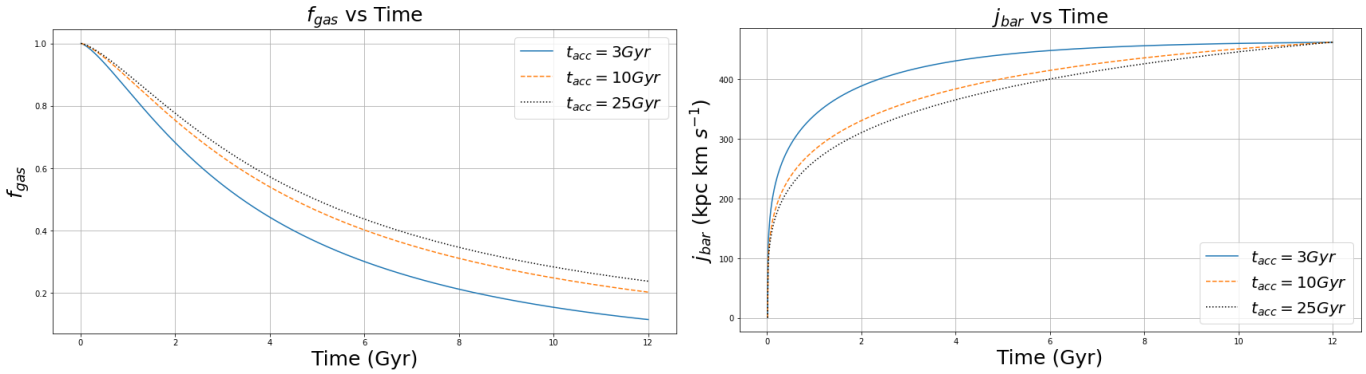

(a) Gas fraction versus time

(b) Specific angular momentum versus time

Figure 8: Gas fraction (8a) and specific angular momentum (8b) against time for three different values of t_{acc}. This model has $M_{bar}(t_0) = 10^{10} M_\odot$ and $r_{acc} = 1.9kpc$

Note that, although 8 shows the global f_{gas} and j_{bar} for the entire time evolution (from $t = 0$ to $t = t_o$), our interest is in the results obtained for the final time ($t = t_o$). For this time value we will later do a direct comparison with the observations.

As can be seen above, varying the accretion timescale induces a variation in f_{gas} but does not lead to a variation in j_{bar} at t_o. In physical terms, the larger the accretion timescale, the larger the gas fraction obtained. This occurs since, for a higher accretion timescale, the galaxy is accreting gas as well as forming stars over a longer period of time. As a result, f_{gas} is larger for $t_{acc} = 25$Gyr than for $t_{acc} = 10$, 3 Gyr at every point in time.

However, whilst f_{gas} changes in time depending on the different accretion timescale, j_{bar} does not show the same trend. Figure 8b shows that regardless of the value for t_{acc}, j_{bar} converges to the same value at time 12 Gyr. Also, Figure 8b shows that j_{bar} evolves up to a particular value at 12 Gyr in a different way depending on the accretion timescale. As already mentioned, the specific angular momentum is defined by equation 19. Hence j_{bar} depends on both the parameter Σ_{bar} and the v_{rot}. However, for an exponential disc rotating at v_{rot} constant with radius, the baryonic specific angular momentum can be rewritten and is defined by

$$j_{bar} = 2\, r_{disc}\, v_{rot}\,, \tag{22}$$

where r_{disc} is the scale radius of the exponential profile (Obreschkow, Glazebrook, et al. (2016)). Because in this model the exponential scale-length for gas accretion is assumed constant with time, the evolution of j_{bar} from time 0 to 12 Gyr is dictated by the evolution of the rotational velocity. For a smaller accretion timescale, the baryonic mass evolves at a faster rate and hence by using the baryonic Tully-Fisher relation so does the rotational velocity. Since $j_{bar} \propto v_{rot}$,

in Figure 8b it can be observed that j_{bar} converges faster at a smaller accretion timescales. Ultimately, the conclusion reached by altering t_{acc} whilst keeping r_{acc} constant is that within the assumptions of this particular model, the accretion history is not a suitable candidate to drive the observed $f_{gas} - j_{bar}$ correlation.

3.3 Varying the radial scale length of the accretion history

The next step was hence to check whether changing the other parameter of the model (r_{acc}), while keeping t_{acc} constant, yields the observed correlation between f_{gas} and j_{bar} for a fixed $M_{bar}(t_0) = 10^{10} M_\odot$. As explained in Section 2.3, the values 0.95kpc, 1.9kpc and 3.8kpc were chosen for r_{acc} following equation 14 and halving and doubling the value obtained. Figure 9 shows the time evolution of f_{gas} and j_{bar} for the various values of r_{acc} obtained for t_{acc} of 10 Gyr. However, a similar trend was observed when considering a constant accretion timescale of 3 and 25 Gyr.

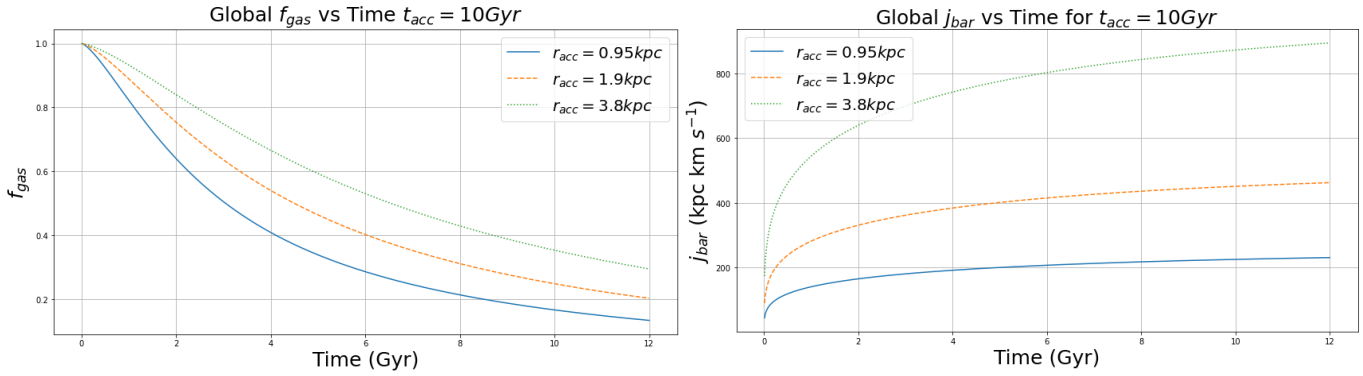

(a) Gas fraction versus time

(b) Specific angular momentum versus time

Figure 9: Gas fraction (9a) and specific angular momentum (9b) against time for three different radial scale lengths of the accretion profile at an accreting timescale of 10 Gyr. This model has $M_{bar}(t_0) = 10^{10} M_\odot$ and $t_{acc} = 10Gyr$

As can be seen in Figure 9, both f_{gas} and j_{bar} are observed to increase with increasing r_{acc}. This ties with what was discussed in Section 3.1.2 concerning the SFE. For a fixed baryonic mass, we observe that a larger r_{acc}, leads to a gas disc that is more extended, and so there is more gas present in the outer regions, which are less efficient at forming stars leading to a larger gas fraction (Mancera-Piña et al. (2021) ; Leroy et al. (2008)) Due to an increased amount of gas in the outer regions of a galaxy with larger r_{acc}, there is also more star formation, and so the stellar disc is also more extended. Combining the two yields an overall extended baryonic disc resulting in higher specific angular momenta. As a result a positive correlation is observed between f_{gas} and j_{bar}.

Hence, within the many assumptions underlying this model, the plots in Fig-

ure 9 seem to be indicating that the angular momentum of the accreting gas, parametrized by its radial scale length is a possible physical driver for the observed correlation.

3.4 Comparison with observed data

In this subsection a quantitative comparison between the model and the best-fit relation found from real data by Mancera-Piña et al. (2021) will be shown. Figure 10 depicts the model described by equation 3 which was obtained by Mancera-Piña et al. (2021). Using the coefficients for the baryon relation taken from their work, equation 3 can be rewritten as

$$\log\left(\frac{j_{bar}}{kpc\,kms^{-1}}\right) = 0.73\,\log\left(\frac{M_{bar}}{M_{\odot}}\right) + 0.46\,\log\left(f_{gas}\right) - 4.25\,. \tag{23}$$

For a range of f_{gas}, this model was plotted for $\log\left(\frac{M_{bar}}{M_{\odot}}\right) = 8$ (Figure 10a) and for $\log\left(\frac{M_{bar}}{M_{\odot}}\right) = 10$ (Figure 10b) and is labeled "Obs" in Figure 10. On the same plots, I have also placed the data points obtained from my model for a constant accretion timescale, and three values for r_{acc}, determined following the method described in Section 2.3. As can be seen, for both present day baryonic masses, the observed relation goes through the points obtained from my model, as the two have a similar normalisation. It is evident that varying the the radial scale length of accretion history whilst keeping the accretion timescale constant drives a relation in the desired direction.

However, for fixed t_{acc} a steeper slope than that of the fit by Mancera-Piña et al. (2021), whose slope has a value of $\beta_{bar} = 0.46 \pm 0.05$, is obtained. As the accretion timescale increases the slope obtained also increases from 1.34 (for $t_{acc} = 3Gyr$) to 2.01 (for $t_{acc} = 25Gyr$) in plot 10a, and from 1.26 to 1.86 in plot 10b. As a result, if one assumes a fixed accretion timescale, a smaller value of t_{acc} would predict a slope closer to that of the relation described by equation 23.

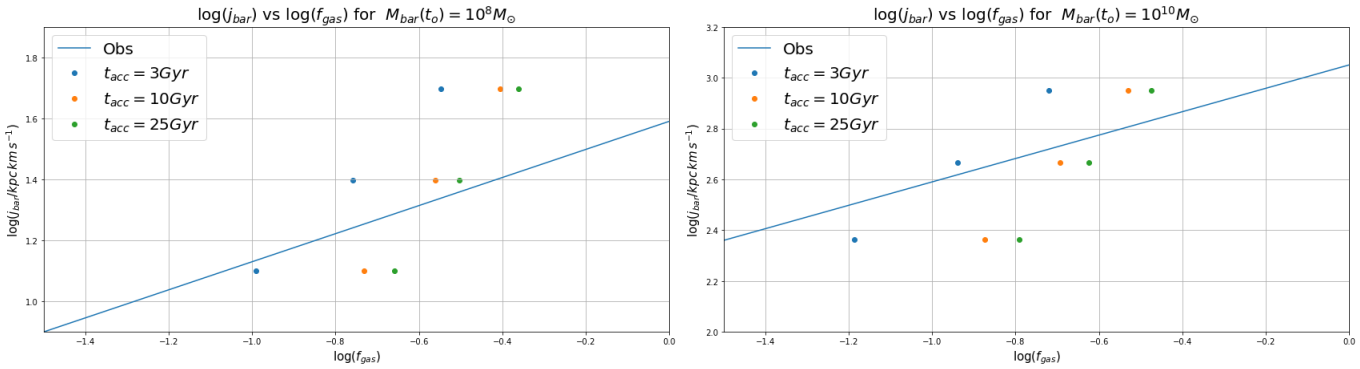

(a) (b)

Figure 10: j_{bar} against f_{gas} in the logarithmic scale for $M_{bar}(t_0) = 10^8 M_\odot$ (10a) and $10^{10} M_\odot$ (10b). The data points are color coded for three accretion timescales with three values of r_{acc} obtained using the method described in Section 2.3

Furthermore, at fixed t_{acc} , the agreement between my model and the data is better for high M_{bar} than for small M_{bar}. It is also important to note that t_{acc} and r_{acc} could also be varying simultaneously. In particular, Figure 10 seems to suggest that creating a model in which t_{acc} and r_{acc} are correlated would predict a slope closer to the observed value. This will also be discussed further in Section 4.1 and is something that could be worth looking into in the future.

3.4.1 Investigating the full $M_{bar} - j_{bar} - f_{gas}$ relation

Next the $M_{bar} - j_{bar} - f_{gas}$ relation was analysed in its entirety by plotting a graph of the specific angular momentum against different baryonic masses in the logarithmic scale for time t_o = 12 Gyr with points color coded according to f_{gas}. For constant accretion timescales of 3 and 25 Gyr, there is some agreement between my model and the data as in Figure 11.

Similarly to observations, the results obtained using my model for an exponential accretion history show that j_{bar} increases with increasing M_{bar}. Also, at fixed M_{bar}, there is an observed increase in j_{bar} as f_{gas} increases. By overlaying lines with constant f_{gas} from the best-fit relation found by Mancera-Piña et al. (2021) (equation 23), a direct comparison between my model and real data can be made. Figure 11 shows how there is a broad quantitative agreement across a large range of the parameter space, as can be seen by the fact that the lines with a constant f_{gas} overlap with points from my model of a similar color, signifying that the two somewhat agree also in their gas fraction value.

However, all the data points produced using my model for $t_{acc} = 3$Gyr have values for the gas fraction lying within the range 0.05 and 0.31. Taking a larger accretion timescale, such as that of 25 Gyr yields larger values for gas fraction however these are still within the range of 0.13 and 0.43. This is a much narrower

range of f_{gas} in the observed galaxies whose f_{gas} range from 0 to 1.

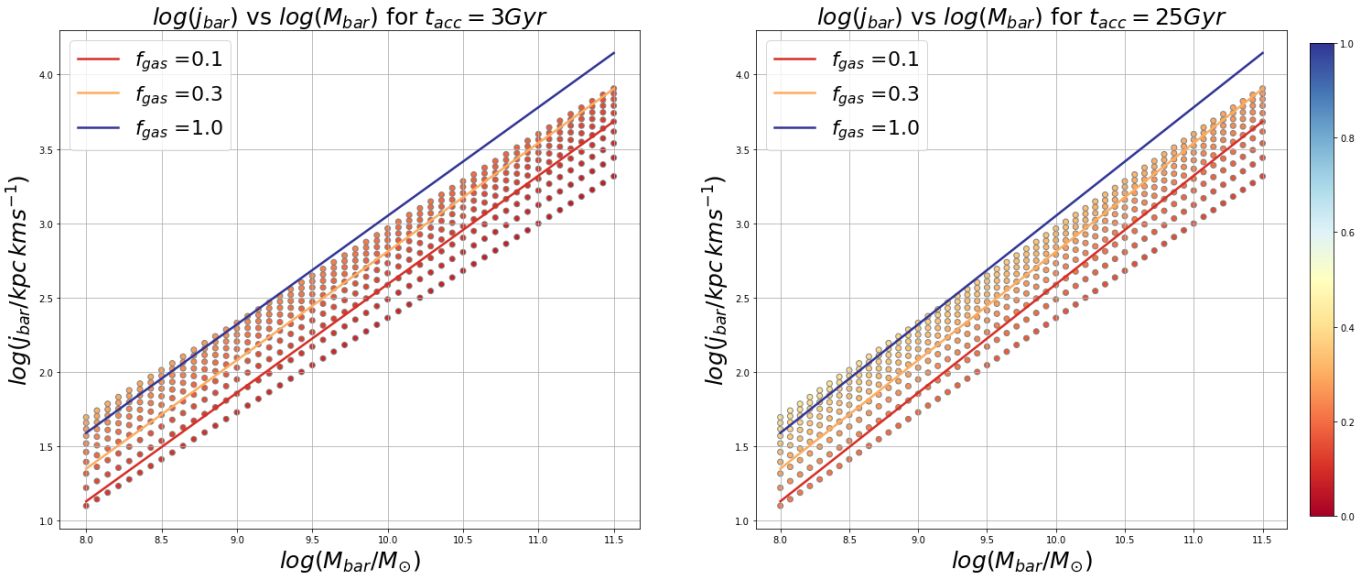

Figure 11: Specific angular momentum against masses in the logarithmic scale for two different accretion timescales. Each data point is color-coded depending on its corresponding value of gas fraction and are compared with three lines of constant f_{gas} using equation 23

When comparing my data points with the lines of constant f_{gas} found using equation 23 from work by Mancera-Piña et al. (2021), there is an offset in both normalisation and the slope. And in both plots, the lines of constant f_{gas} do not entirely coincide with the data points having the same f_{gas} value. Following this, in the future, it could be of interest to observe how this figure would change by treating t_{acc} and r_{acc} in a correlated manner, and more improvements and future work will be discussed in Section 4.2.

4 Discussion

In this section I will discuss what the interpretation of the results are (Section 4.1), as well as the limitations and directions for future work (Section 4.2). All quantities mentioned are evaluated at the present time t = t_o.

4.1 Interpretation of Results

The results of varying the accretion timescale (t_{acc}) and the radial scale length of the accretion profile (r_{acc}) in our simple galaxy evolution model with exponential accretion are shown in sections 3.2 and 3.3, respectively. When analysing different values for t_{acc} for a constant r_{acc}, a variation in f_{gas} was induced, but j_{bar} remained a constant at t_o. As a result, it can be concluded that within the assumptions of this model, variations in t_{acc} cannot explain the observed correlation between f_{gas} and j_{bar} at fixed M_{bar}. However, given the simplicity of the model developed, this particular conclusion could have been a consequence of our particular assumptions and the result should be checked again with different models.

On the other hand, the results in Section 3.3 show that, in this model, variations in r_{acc} at constant t_{acc} lead to a variation in both f_{gas} and j_{bar} and so this parameter is a suitable candidate to explain the observed correlation between f_{gas} and j_{bar} at fixed M_{bar}. This positively correlated variation in f_{gas} and j_{bar} agrees qualitatively with the observations by Mancera-Piña et al. (2021). This can be easily understood, considering that variations in r_{acc} induce variations in the extension of a galaxy disc, which leads to an increase in the baryonic specific angular momentum as well as the extent of the baryonic distribution in the outer regions of the disc. Due to the fact that the SFE is lower at larger radii, less stars form resulting in an increased gas fraction. Hence, our model supports the idea that the observed $M_{bar} - j_{bar} - f_{gas}$ relation is related to the star formation efficiency being lower in the outer regions of the disc.

According to equation 22, r_{acc} is correlated to the angular momentum of the accreting gas. As a result, the physical interpretation of our results is that the candidate physical driver of the observed correlation between j_{bar} and f_{gas} is the angular momentum of the accreting gas. However, possible refinements to this simple picture will be further discussed in Section 4.2.1 for future work and improvement of our model.

Figure 10 showed how the data points obtained from my model are in approximate agreement with the observed relation (equation 23) for a constant M_{bar}. Whilst the slope and normalisation for a fixed t_{acc} are not in exact accordance with the data from Mancera-Piña et al. (2021), the observed relation goes through the points obtained from my model. Hence taking into account the assumptions

taken in this model, this agreement is acceptable. Inspection of Figure 10 suggests that a better agreement could be found by exploring a model in which neither t_{acc} nor r_{acc} are held constant, but instead assumed to vary in a correlated way. The exploration of this possibility is left for future work.

Lastly, the full $M_{bar} - j_{bar} - f_{gas}$ relation produced by my model was analysed in Section 3.4.1. The results obtained were compared to the observed relation given by equation 23 for different values of fixed f_{gas}. Figure 11 shows how for a large part of the $M_{bar} - j_{bar}$ plane, the model and data show similar values of f_{gas} which is indicated by the colors of each plot. However, the model does not reproduce the observations in the regime of high f_{gas}. In particular, the model does not produce galaxies with f_{gas} larger than 0.31 for $t_{acc} = 3$Gyr and 0.43 for $t_{acc} = 25$Gyr, in contrast with the observations.

Since it was concluded that an increase in r_{acc} is correlated to an increase in the gas fraction, one possible solution to the small range of obtained f_{gas} values could be obtained by using a larger range of r_{acc}. Whilst this could be looked into using different models, the range r_{acc} used cannot be increased too much as this would imply a corresponding change in the scale length of the stellar disc (r_*), although this point was not investigated quantitatively in this thesis. Also, from Figure 10 it is evident that a larger range of r_{acc} would not improve our model in the desired way since, increasing or decreasing r_{acc} would have no effect on the slope or normalisation of the results. As a result using a larger range of r_{acc} is not expected to be a final solution, and other, more promising solutions will be discussed in Section 4.2.

Whilst the model is very simple in nature, the obtained trend in the $M_{bar} - j_{bar} - f_{gas}$ relation is qualitatively correct. For the first time with a quantitative model, this research project showed that a positive correlation between j_{bar} and f_{gas} at fixed M_{bar} can arise as a consequence of a radially varying SFE. Any deviations from the observed relation are most likely due to a combination of imperfect assumptions, in particular on the accretion history and the star formation law, as discussed in more detail Section 4.2. However, despite the inaccuracies, the assumptions taken made it possible to propose a suitable candidate responsible for the $M_{bar} - j_{bar} - f_{gas}$ relation under such simple conditions.

4.2 Limitations and Possible Improvements

Here I will talk about how the model could be improved to include more realistic assumptions which may lead to a better agreement with the observed data.

4.2.1 Changing Assumptions on the Accretion Profile

Throughout this project, it was assumed that the accretion profile is exponential in both time and radius, with scale-length independent on time and value of r_{acc} taken from the relation by Wu (2018) (equation 14). One possible improvement mentioned in Section 4.1, would be to treat t_{acc} and r_{acc} in a correlated manner as suggested before.

Another point of interest to explore different mass - size relations. One possibility to consider could be to utilise the relation between stellar mass(M_*) and the radius containing half of the galaxy's light, known as the effective half-light radius (R_e), for instance as derived by Lange et al. (2015). The use of this relation would require some modifications to our formalism, as we would then need to use the stellar mass, instead of the baryonic mass, as an independent variable. It could however be an interesting alternative to look into in the future.

The most important assumption to be revisited is perhaps that our galaxy evolution model followed an accretion history that is separable in space and time. In particular, the radial scale length of the accretion profile was taken to be constant with time. However, as already discussed in Section 1.1.1 and 4.1, the tidal torque theory (TTT) states that the angular momentum of the accreting gas is an increasing function of time, and despite this behaviour is partly captured by our model as a consequence of the evolution of v_{rot} (see for instance Section 3.2 and Figure 8), also r_{acc} is expected to evolve. Hence, one natural improvement to be done on this model is to allow this parameter to evolve in time, for instance in the form $r_{acc}(t) = r_o + bt$ where b is a constant.

Due to time constraints, the evolution of r_{acc} was not taken into account throughout this research project and yet the results obtained are still meaningful. We show that even when treating the accretion history's spatial and time dependence separately, the variations in radial scale length of the accretion history is correlated to variations in f_{gas} and j_{bar} for a constant M_{bar}. We also note that although the model developed throughout this research project is not inside-out in the accretion, as it is likely the case in reality, we still observe some moderate increase in the radial extent of Σ_* as seen in Figure 4. This, as discussed in Section 3.1.2 is also a consequence of a lower SFE in the outer regions of the galaxy.

4.2.2 Changing the Rotation Curve

The assumptions made on the rotation velocity were discussed in Section 2.6 and included the independence of v_{rot} on radius, the non-evolving baryonic Tully-Fisher relation (BTFR) (equation 20) and assuming that gas and stars rotate at the same velocity.

One potential improvement could therefore be to remove the approximation

of a flat rotation curve. However, changes to the rotation curve are not expected to change the resulting values for the baryonic specific angular momentum significantly enough as any corrections would likely be too small. As already pointed out in Section 2.6 (equation 19), we observe a dependency on R^2 in the numerator which shows that in determining j_{bar}, v_{rot} becomes significantly more important at larger radii of the galactic disc. In these regions the rotational velocity is more or less constant and so assuming a flat rotation curve is a suitable assumption and introduces a very small error (Vukcevic (2021)).

In assuming that gas and stars have the same v_{rot}, asymmetric drift was not taken into account. This phenomenon describes the tendency for the mean v_{rot} of a population of stars to lag behind the v_{rot} of the gas. Correcting for this would involve taking into account the asymmetric drift velocity given by

$$v_{AD}^2 = \sigma_z^2 \frac{3\,R}{2\,R_d} \tag{24}$$

Taking this phenomenon into account in approximating j_{bar}, and assuming that the stellar velocity dispersion in the z direction, σ_z, varies exponentially with radius according to

$$\sigma_z = \sigma_0\, e^{-\frac{R}{2\,R_d}}, \tag{25}$$

where R_d is the scale-length of the galaxy disc, would introduce a correction smaller than 5% in j_{bar}, which is not a significant enough change (Posti et al. (2018)).

4.2.3 Changing the Star Formation Law

Despite its popularity and successes, it is also known that the Kennicutt-Schmidt (K-S) law (equation 4) is not perfect. In this subsection the effects of changing the star formation law will be considered in light of possible future work.

One indication that a different SFL could have been used is in the very low values for the gas fraction obtained, ranging only between 0.05 and 0.43, which is visible in Figure 10. This is in contrast with the observation that dwarf galaxies ($10^7 M_\odot < M_{bar} < 10^9 M_\odot$) typically have larger gas fractions as can be seen in Figure 2. Therefore, in our model, the dwarf galaxies appear to be forming an excess of stars. One possible solution could be to consider a different star formation law which predicts lower levels of star formation for low-mass galaxies. This possibility also has an independent observational motivation. For instance Gatto et al. (2013) have shown that dwarf galaxies lie along a steeper relation described by the equation

$$\Sigma_{SFR} = (2.13 \pm 0.6)\ 10^{-5} \cdot \Sigma_{gas}^{2.47}\,, \tag{26}$$

where the Σ_{SFR} is in $M_\odot\, yr^{-1}\, kpc^{-2}$ and Σ_{gas} in $M_\odot\, pc^{-2}$. This relation is plotted in Figure 12 for direct comparison with the standard Kennicutt–Schmidt relation for disc galaxies, and whilst the two agree at $\Sigma_{gas} \approx 10 M_\odot pc^{-2}$, it is apparent that

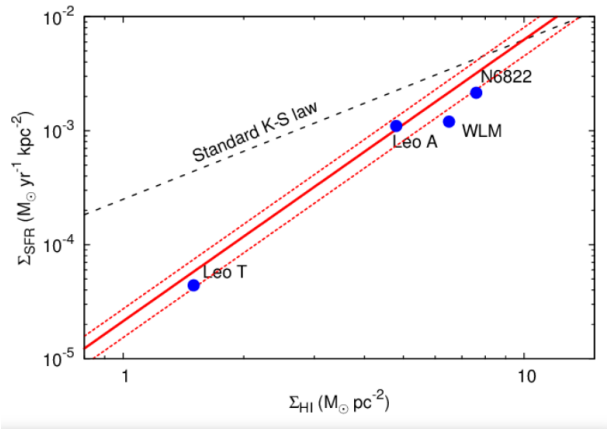

Figure 12: Plot showing the standard K-S law (black dashed line) and the relation valid for a small sample of dwarf galaxies (red solid line) described by equation 26 along with its error bar of 1 σ (red dashed lines) taken from Gatto et al. (2013). The solid blue dots represent four dwarf irregular galaxies found in the Local Group having different surface densities of gas and star formation rate.

the relation described by equation 26 seems to be in better agreement with the observations, at least for these four dwarf galaxies.

As an experiment, the SFL proposed by Gatto et al. (2013) (equation 26) was applied to the model developed in this project to see whether this leads to an improvement to the results of Figure 10. The results obtained when utilising this SFL instead of the K-S law can be seen in Figure 13.

As suspected, Figure 13 shows how using the SFL dictated by equation 26 instead of the K-S law resulted in overall larger values for f_{gas} than obtained previously. And similarly to the results shown in Figure 11, for a larger the accretion timescale the values of the gas fraction were larger than those obtained for a lower t_{acc}. However, when comparing with the data from Mancera-Piña et al. (2021) for a fixed gas fraction it is evident there is less agreement when adopting the SFL given by equation 26 than when using the standard K-S law as in Figure 10. Therefore using the alternative SFL proposed by Gatto et al. (2013) did not improve the agreement between my model and the observations.

4.2.4 Volumetric Star Formation Laws

Up to this point, all SFLs considered throughout this thesis (the standard K-S law, and the SFL by Gatto et al. (2013)) are based on surface densities. Whilst SFLs based on surface densities are somewhat easier to use in galaxy evolution models, they often implicitly assume galaxy discs with a constant scale height. Meanwhile, observations show that regardless of the galaxy type, a galaxy's disc increases in thickness at larger distances from the galactic center (Bacchini et al. (2020)). As a result, a constant scale height is not a good representation of

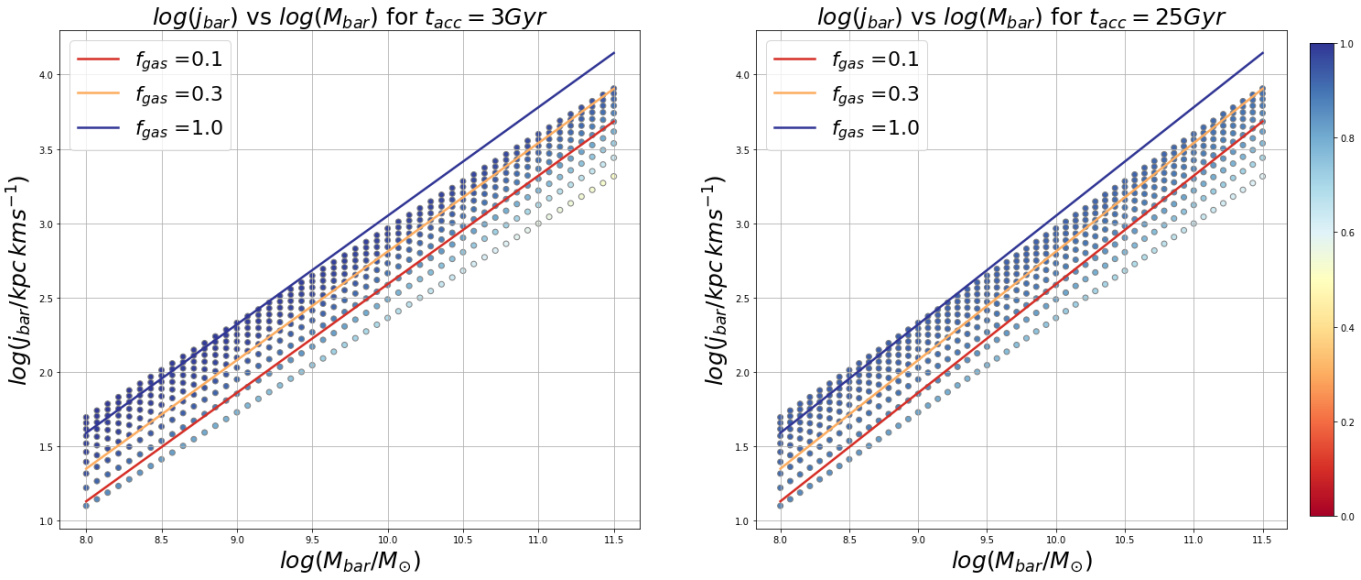

Figure 13: Specific angular momentum against mass in the logarithmic scale following the SFL described in equation 26 for two values of t_{acc}. Each data point is color coded depending on its corresponding gas fraction value and 3 lines of fixed f_{gas} using equation 20 from Mancera-Piña et al. (2021) were overlayed on the plots for direct comparison

reality and is an inaccurate approximation to adopt.

Bacchini et al. (2019) have shown that volumetric star formation (VSF) laws can better explain the star formation across a wide range of galaxy mass and gas surface density, by taking into account the effect of disc flaring, whilst also producing a much smaller scatter than two-dimensional SFLs. Hence, improvement on this galaxy evolution model could be made in the future by using a volumetric star formation (VSF) law.

Bacchini et al. (2019) found in particular a VSF of the form

$$\rho_{SFR} = A\,\rho_{gas}^{\alpha}\,, \tag{27}$$

were ρ_{SFR} is the SFR per unit volume, ρ_{gas} is the volume density of the gas including neutral and molecular gas, and A and α are constants dictating the normalisation and slope respectively. The fact that the SFL is better described by volume (rather than surface) densities is also in agreement with an idea originally proposed by Schmidt (1959). In order to derive the volume densities, Bacchini et al. (2019) estimate the gas velocity dispersion and assumed that the gas disc is in hydrostatic equilibrium.

By using a VSF law in a future extension of this work, the volume densities of gas and SFR could be reconstructed, and the effect this produces on the $M_{bar} - j_{bar} - f_{gas}$ relation could be investigated. Despite having the advantage of being valid for a variety of galaxy types and densities, using a VSF law also comes with various challenges, including making approximations for the the galaxy's

gravitational potential and the gas's velocity dispersion $\sigma(R)$, which were beyond the scope of this bachelor thesis.

5 Summary and Conclusion

Throughout this thesis we have built a simple galaxy evolution model for disc galaxies with the aim of reproducing the baryonic $j - M - f_{gas}$ scaling relation found by Mancera-Piña et al. (2021). The model was based on the assumptions of having an exponential accretion profile in both space and time, and that star formation obeys the Kennicutt–Schmidt (K-S). The stars and gas rotate at the same velocity v_{rot} determined by baryonic Tully-Fisher relation (BTFR).

For each value of the present-day baryonic mass ($M_{bar}(t_o)$), the model is defined by two parameters: the radial scale length of the accretion profile and the accretion timescale, denoted by r_{acc} and t_{acc} respectively. The variations induced in j_{bar} and f_{gas} as a result of varying r_{acc} and t_{acc} for a fixed M_{bar} were then explored. The results were then compared to the best fit relation found from real data by Mancera-Piña et al. (2021).

It was seen that for a fixed $M_{bar}(t_o)$, and fixed r_{acc}, variations in t_{acc} did not lead to a correlated variation in j_{bar} and f_{gas} and therefore cannot explain the observations. On the other hand, varying r_{acc} whilst keeping t_{acc} constant, a positively correlated variation in j_{bar} and f_{gas} for a fixed $M_{bar}(t_o)$ was obtained. It was hence concluded that, within the assumptions of our model, r_{acc} could be responsible for driving the observed $M_{bar} - j_{bar} - f_{gas}$ relation.

When analysing the full $M_{bar} - j_{bar} - f_{gas}$ relation for a range of galaxies with baryonic masses ranging between $10^8 M_\odot - 10^{11.5} M_\odot$, we achieved a qualitative agreement between the results of my model and the observed relation. In particular j_{bar} increases with increasing M_{bar} and furthermore, for a fixed M_{bar} , the model predicts an increase in j_{bar} when f_{gas} increases. The result supports the idea that the positive correlation between j_{bar} and f_{gas} is driven by the SFE being lower on outer regions of the galaxy, although some quantitative discrepancies between the model predictions and the observations still remain. Among directions for future improvement, one possibility could be treating r_{acc} and t_{acc} in a correlated way. Other propositions for future work include considering a dependence of r_{acc} on time or replacing the K-S law with a volumetric star formation law.

6 Acknowledgements

The submission of this thesis marks the end of the 3 month journey I took diving deeper into one of the most fundamental galaxy scaling relations. A journey that has thought me immensely, and one that I could not have completed successfully were it not for the great patience of my supervisors Filippo Fraternali and Gabriele Pezzulli. From the bottom of my heart I would like to sincerely thank you both for helping me every step of the way. From having to explain concepts numerous times to ensure my understanding, to pushing me to keep trying and working hard despite my occasional struggles in programming. I cannot thank you enough for always being there and replying to my endless emails. I have the utmost level of respect for both of you and am grateful to have had you both as my supervisors.

I would also like to thank one of my best friends Evan Van der Voort, whom without his constant support I would also not have managed to finish this bachelor project. You have been by my side since the first class we had together in first year, and have never stopped being there for me ever since. We've always helped each other, and honestly, I couldn't have asked for a better friend to go through both these last 3 months, and more importantly these last three years. You encouraged me to keep going when studies got overwhelming, and have helped me more times than I can count.

Lastly, I'd like to thank my best friend Michela, my sister and parents. Although you are physically miles away from me, you were always a phone call away. Mum and Dad thank you for pushing me every step of the way and for believing in me always. Michela, I could not have finished this project were it not for the random phone calls in the middle of the night. And Nikita, I've always looked up to you, and always will. Thank you for always giving me the best of advice.

References

Bacchini, C et al. (2019). "Volumetric star formation laws of disc galaxies". In: *A&A* 622, A64. DOI: 10.1051/0004-6361/201834382. URL: https://doi.org/10.1051/0004-6361/201834382.

Bacchini, C et al. (Dec. 2020). "The volumetric star formation law for nearby galaxies. Extension to dwarf galaxies and low-density regions". In: 644, A125, A125. DOI: 10.1051/0004-6361/202038962.

Bennett, C. L. et al. (Sept. 2013). "NINE-YEAR iWILKINSON MICROWAVE ANISOTROPY PROBE/i (iWMAP/i) OBSERVATIONS: FINAL MAPS AND RESULTS". In: *The Astrophysical Journal Supplement Series* 208(2), p. 20. DOI: 10.1088/0067-0049/208/2/20. URL: https://doi.org/10.1088/0067-0049/208/2/20.

Chabrier, Gilles (July 2003). "Galactic Stellar and Substellar Initial Mass Function". In: 115(809), pp. 763–795. DOI: 10.1086/376392.

Cimatti, Fraternali, and Nipoti (2019). *Introduction to Galaxy Formation and Evolution: From Primordial Gas to Present-Day Galaxies*. Cambridge University Press.

Faber, S. M. and J. S. Gallagher (Jan. 1979). "Masses and mass-to-light ratios of galaxies." In: 17, pp. 135–187. DOI: 10.1146/annurev.aa.17.090179.001031.

Fall, S. M. (Jan. 1983). "Galaxy formation - Some comparisons between theory and observation". In: *Internal Kinematics and Dynamics of Galaxies*. Ed. by E. Athanassoula. Vol. 100, pp. 391–398.

Fall, S. Michael and G. Efstathiou (Nov. 1980). "Formation and rotation of disc galaxies with haloes". In: *Monthly Notices of the Royal Astronomical Society* 193(2), pp. 189–206. ISSN: 0035-8711. DOI: 10.1093/mnras/193.2.189. eprint: https://academic.oup.com/mnras/article-pdf/193/2/189/2939800/mnras193-0189.pdf. URL: https://doi.org/10.1093/mnras/193.2.189.

Fernández Lorenzo et al. (2011). "Evolution of the fundamental plane of 0.2 early-type galaxies in the EGS". In: *A&A* 526, A72. DOI: 10.1051/0004-6361/201015368. URL: https://doi.org/10.1051/0004-6361/201015368.

Frankel, Neige et al. (Oct. 2019). "The Inside-out Growth of the Galactic Disk". In: *The Astrophysical Journal* 884(2), p. 99. DOI: 10.3847/1538-4357/ab4254. URL: https://doi.org/10.3847%2F1538-4357%2Fab4254.

Fraternali (2017). "Gas Accretion via Condensation and Fountains". In: *Gas Accretion onto Galaxies*. Springer International Publishing, pp. 323–353. DOI: 10.1007/978-3-319-52512-9_14. URL: https://doi.org/10.1007%2F978-3-319-52512-9_14.

Fraternali, Filippo and Matteo Tomassetti (Nov. 2012). "Estimating gas accretion in disc galaxies using the Kennicutt–Schmidt law". In: *Monthly Notices of the Royal Astronomical Society* 426(3), pp. 2166–2177. ISSN: 0035-8711. DOI: 10.1111/j.1365-2966.2012.21650.x. URL: https://doi.org/10.1111/j.1365-2966.2012.21650.x.

Gatto, Andrea et al. (2013). "Unveiling the corona of the Milky Way via ram-pressure stripping of dwarf satellites". In: *Monthly Notices of the Royal Astronomical Society* 433, pp. 2749–2763.

Hubble, E. P. (Dec. 1926). "Extragalactic nebulae." In: 64, pp. 321–369. DOI: 10.1086/143018.

Kennicutt (May 1998). "The Global Schmidt Law in Star-forming Galaxies". In: 498(2), pp. 541–552. DOI: 10.1086/305588.

Kennicutt and Evans (Sept. 2012). "Star Formation in the Milky Way and Nearby Galaxies". In: 50, pp. 531–608. DOI: 10.1146/annurev-astro-081811-125610.

Kereš, Dušan et al. (May 2009). "Galaxies in a simulated ΛCDM Universe - I. Cold mode and hot cores". In: 395(1), pp. 160–179. DOI: 10.1111/j.1365-2966.2009.14541.x. arXiv: 0809.1430 [astro-ph].

Komatsu, E. et al. (2009). "Five-year wilkinson microwave anisotropy probe observations: Cosmological interpretation". In: *Astrophysical Journal, Supplement Series* 180(2), pp. 330–376. ISSN: 0067-0049. DOI: 10.1088/0067-0049/180/2/330.

Kroupa, Pavel, Christopher A. Tout, and Gerard Gilmore (June 1993). "The Distribution of Low-Mass Stars in the Galactic Disc". In: 262, pp. 545–587. DOI: 10.1093/mnras/262.3.545.

Kurapati, Sushma et al. (May 2018). "Angular momentum of dwarf galaxies". In: *Monthly Notices of the Royal Astronomical Society* 479(1), pp. 228–239. ISSN: 0035-8711. DOI: 10.1093/mnras/sty1397. URL: https://doi.org/10.1093/mnras/sty1397.

Lange, Rebecca et al. (Jan. 2015). "Galaxy And Mass Assembly (GAMA): mass–size relations of z &lt 0.1 galaxies subdivided by Sérsic index, colour and morphology". In: *Monthly Notices of the Royal Astronomical Society* 447(3), pp. 2603–2630. DOI: 10.1093/mnras/stu2467. URL: https://doi.org/10.1093%2Fmnras%2Fstu2467.

Leroy, Adam K. et al. (Dec. 2008). "The Star Formation Efficiency in Nearby Galaxies: Measuring Where Gas Forms Stars Effectively". In: 136(6), pp. 2782–2845. DOI: 10.1088/0004-6256/136/6/2782. arXiv: 0810.2556 [astro-ph].

López, Pablo, Manuel E Merchán, and Dante J Paz (Mar. 2019). "Deviations from tidal torque theory: environment dependences on halo angular momentum growth". In: *Monthly Notices of the Royal Astronomical Society* 485(4), pp. 5244–5255. DOI: 10.1093/mnras/stz762. URL: https://doi.org/10.1093%2Fmnras%2Fstz762.

Mancera Piña et al. (Mar. 2021). "The baryonic specific angular momentum of disc galaxies". In: 647, A76, A76. DOI: 10.1051/0004-6361/202039340. arXiv: 2009.06645 [astro-ph.GA].

Mancera-Piña, Pavel E. et al. (2021). "A tight angular-momentum plane for disc galaxies". In: *A&A* 651, p. L15. DOI: 10.1051/0004-6361/202141574. URL: https://doi.org/10.1051/0004-6361/202141574.

McGaugh, Stacy S. (Jan. 2012). "THE BARYONIC TULLY–FISHER RELATION OF GAS-RICH GALAXIES AS A TEST OF {$upLambda$". In: *The Astronomical*

Journal 143(2), p. 40. DOI: 10.1088/0004-6256/143/2/40. URL: https://doi.org/10.1088%2F0004-6256%2F143%2F2%2F40.

Obreschkow, D. and K. Glazebrook (Mar. 2014). "Fundamental Mass-Spin-Morphology Relation Of Spiral Galaxies". In: 784(1), 26, p. 26. DOI: 10.1088/0004-637X/784/1/26. arXiv: 1312.4543 [astro-ph.GA].

Obreschkow, D., K. Glazebrook, et al. (June 2016). "Angular momentum regulates atomic gas fractions of galactic disks". In: *Astrophysical Journal Letters* 824(2). ISSN: 2041-8205. DOI: 10.3847/2041-8205/824/2/L26. URL: https://www.osti.gov/biblio/22868978.

Ostriker, J. P. and P. J. E. Peebles (Dec. 1973). "A Numerical Study of the Stability of Flattened Galaxies: or, can Cold Galaxies Survive?" In: 186, pp. 467–480. DOI: 10.1086/152513.

Pagel, Bernard E. J. (1997). *Nucleosynthesis and Chemical Evolution of Galaxies*.

Peebles, P. J. E. (Feb. 1969). "Origin of the Angular Momentum of Galaxies". In: 155, p. 393. DOI: 10.1086/149876.

Pezzulli, Gabriele and Filippo Fraternali (Oct. 2016). "Accretion, radial flows and abundance gradients in spiral galaxies". In: *Monthly Notices of the Royal Astronomical Society* 455. DOI: 10.1093/mnras/stv2397.

Pezzulli et al. (Aug. 2015). "The instantaneous radial growth rate of stellar discs". In: 451(3), pp. 2324–2336. DOI: 10.1093/mnras/stv1077. arXiv: 1505.03544 [astro-ph.GA].

Posti, Lorenzo et al. (Dec. 2020). "The impact of the halo spin-concentration relation on disc scaling laws". In: 644, A76, A76. DOI: 10.1051/0004-6361/202038474. arXiv: 2010.09727 [astro-ph.GA].

Posti, Lorenzo et al. (2018). "The angular momentum-mass relation: a fundamental law from dwarf irregulars to massive spirals". In: *A&A* 612. DOI: 10.1051/0004-6361/201833091. URL: https://doi.org/10.1051/0004-6361/201833091.

Prantzos, N. (2008). "An Introduction to Galactic Chemical Evolution". In: *EAS Publications Series* 32, pp. 311–356. DOI: 10.1051/eas:0832009. URL: https://doi.org/10.1051%2Feas%3A0832009.

Romanowsky and Fall (Nov. 2012). "ANGULAR MOMENTUM AND GALAXY FORMATION REVISITED". In: *The Astrophysical Journal Supplement Series* 203(2), p. 17. DOI: 10.1088/0067-0049/203/2/17. URL: https://doi.org/10.1088%2F0067-0049%2F203%2F2%2F17.

Salpeter, E. E. and H. A. Bethe (Dec. 1951). "A Relativistic Equation for Bound-State Problems". In: *Physical Review* 84(6), pp. 1232–1242. DOI: 10.1103/PhysRev.84.1232.

Schmidt, Maarten (Mar. 1959). "The Rate of Star Formation." In: 129, p. 243. DOI: 10.1086/146614.

Slipher, V. M. (Jan. 1913). "The radial velocity of the Andromeda Nebula". In: *Lowell Observatory Bulletin* 2(8), pp. 56–57.

Teodoro, E. M. Di, F. Fraternali, and S. H. Miller (Oct. 2016). "Flat rotation curves and low velocity dispersions in KMOS star-forming galaxie at z$\sim$1". In: 594, A77. DOI: 10.1051/0004-6361/201628315. URL: https://doi.org/10.1051%2F0004-6361%2F201628315.

Tinsley, B. M. (Jan. 1980). "Evolution of the Stars and Gas in Galaxies". In: *Fundamentals of Cosmic Physics* 5, pp. 287–388. DOI: 10.48550/arXiv.2203.02041.

Tully, R. B. and J. R. Fisher (Feb. 1977). "A new method of determining distances to galaxies." In: 54, pp. 661–673.

van der Kruit and Bosma (Nov. 1978). "The rotation curves and orientation parameters of the spiral galaxies NGC 2715, 5033 and 5055." In: 34, pp. 259–266.

van der Kruit, PC and RJ Allen (1978). "The Kinematics of Spiral and Irregular Galaxies". In: *Annual Review of Astronomy and Astrophysics* 16, pp. 103–139. ISSN: 0066-4146. DOI: 10.1146/annurev.aa.16.090178.000535.

Vukcevic, Miroslava (Mar. 2021). "The Spiral Galaxies Flat Rotational Velocity Curve Explained by the Constant Group Velocity of a Nonlinear Density Wave". In: 161(3), p. 118. DOI: 10.3847/1538-3881/abd568.

Wechsler, Risa H. and Jeremy L. Tinker (2018). "The Connection Between Galaxies and Their Dark Matter Halos". In: *Annual Review of Astronomy and Astrophysics* 56(1), pp. 435–487. DOI: 10.1146/annurev-astro-081817-051756.

White, S. D. M. and M. J. Rees (May 1978). "Core condensation in heavy halos: a two-stage theory for galaxy formation and clustering." In: 183, pp. 341–358. DOI: 10.1093/mnras/183.3.341.

Wu, Po-Feng (Feb. 2018). "The scaling relationship between baryonic mass and stellar disc size in morphologically late-type galaxies". In: 473(4), pp. 5468–5475. DOI: 10.1093/mnras/stx2745. arXiv: 1710.06440 [astro-ph.GA].

Zonoozi, Akram Hasani et al. (July 2021). "The Kennicutt–Schmidt law and the main sequence of galaxies in Newtonian and milgromian dynamics". In: *Monthly Notices of the Royal Astronomical Society* 506(4), pp. 5468–5478. DOI: 10.1093/mnras/stab2068. URL: https://doi.org/10.1093%5C%2Fmnras%5C%2Fstab2068.